Efficacy of hydrotalcite Mg-Al membrane based on ghassoul and olive stone in the removal of polyphenols from olive mill wastewater

Safae Allaoui [a,*], Hamid Ziyat [a], Marwa Alaqarbeh [b], Fatima Boukhlifi [a], Najib Tijani [c], Mohammed Naciri Bennani [a,*]

[a] Laboratory of Chemistry-Biology Applied to the Environment, URL-CNRST N°13, Research Team: "Applied Materials and Catalysis" Moulay Ismail University, Faculty of Science, B.P 11201 Zitoune, Meknes, Morocco
[b] Prince Al Hussein bin Abdullah II Academy for Civil Protection, Al-Balqa Applied University, Al-Salt 19117, Jordan
[c] Research Team "Membrane Materials and Separation Processes" Chemistry Department, Faculty of Science, Moulay-Ismaïl University, BP.11201 Zitoune, Meknes 50000, Morocco

ARTICLE INFO

ABSTRACT

The current study aims to fabricate a Hydrotalcite Mg-Al membrane (HT-Gh-OS3) based on Ghassoul and olive stone composite as a microfilter to remove of polyphenols from olive mill wastewater. Also, the results and efficiency of HT-Gh-OS3 membrane was compared with HT-Gh-AC3 membrane used in our previous study where Gh=Ghassoul, OS=olive stone, AC=activated carbon, number 3 relating to the percentage of AC or OS, and HT=Hydrotalcite type MgAlCO3. The hydrotalcite was deposited on the ceramic supports 'Ghassoul' and characterized by Fourier Transform infrared spectroscopy (FTIR), X-ray diffraction (XRD), and Scanning electron microscopy coupled with Energy-dispersive X-ray spectroscopy (SEM/EDX). The diluted OMW with water 40 %, 60 %, and 80 % contains 60 mg/L, 40 mg/L, and 30 mg/L concentrations of polyphenols respectively, which used in the filtration process by the new membrane. The results showed that the olive stone membrane has good porosity and reduced polyphenols by 74 % compared to 61 % by commercial activated carbon membrane. The macroporous structure of olive stones enhances the porosity of the support during sintering, resulting in a higher membrane porosity and better polyphenol reduction. The Hydrotalcite membrane based on the natural material (Ghassoul clay and olive stone) give a good retention of polyphenols of OMWW than the membrane with activated carbon.

1. Introduction

The production of olive oil is one of the most important agricultural industries in many countries, especially Mediterranean basin countries. It generates two waste residues: liquid, called olive mill wastewater (OMWW), and solid olive stone (Bilal et al., 2021; Terral et al., 2021; Berbel et al., 2018). They make a critical environmental issue for all olive oil production countries, particularly in the Mediterranean basin, because their production percentage is largely related to oil production (Di Giacomo et al., 2022; Sciubba et al., 2020). The olive stone has become a proven ingredient in several fields, such as medicines, dietary supplements and cosmetics (Terral et al., 2021; Rodriguez et al., 2008). Olive mill wastewater (OMWW) is one of the most dangerous environmental, health, and agricultural issues, which is highly toxic black-colored water for drinking water, groundwater, and all soil types because it contains high concentrations of heavy metal ions such as (lead, cadmium, arsenic, copper, and manganese), organic substances, phenols, and biological pollutants (Galanakis, 2018). Different methods and techniques were reported in the literature for OMWW treatment such as forward osmosis (Gebreyohannes et al., 2015), supercritical water oxidation (Erkonak et al., 2008), a sequencing batch reactor (Chiavola et al., 2014), photo-Fenton system using artificial ultraviolet light lamps (Galanakis, 2018; García et al., 2017), single electro-coagulation with different electrodes and sequential electro-coagulation/electro-chemical Fenton-based processes (Sani et al., 2020), advanced oxidation process (Flores et al., 2018), using mixed adsorbents of volcanic tuff, natural clay and charcoal (Sciascia et al., 2019; Azzam, 2018). Some of the previous conventional technics are

---

either expensive or difficult to implement. In our case, we utilized a natural clay and OS, disponible and no expensive, for the preparation the membrane (Al Aani et al., 2020), nanofiltration (NF) (Tapia-Quirós et. al, 2022) and microfiltration (MF) using polymeric and commercial membranes. As a result, the current study aims to develop new microfiltration membranes suitable for phenols OMWW removal. The aim of this work is to assess the efficiency of the new membrane (HT-Gh-OS3) for the elimination of the polyphenols from OMWW. To the extent of i) permeate flux; ii) remove of polyphenols and iii) characterization of the membrane microfiltration with SEM before and after the removal process.

2. Materials and instruments

2.1. Materials

The metal salts ($MgCl_2$, $6H_2O$) and ($AlCl_3$, $6H_2O$) with a content of 99 %, sodium hydroxide (NaOH) in pellet form with a purity of 98 %, sodium carbonate (Na_2CO_3) with a purity of 99.9 %, and Folin-Ciocalteu reagent pure, (Ag_2SO_4) silver sulfate, and ($HgSO_4$) mercury sulfate, were provided by LobaChemie. Nitrogen gas was provided by the (Air Liquide Morocco) company, and Gallic acid 1-hydrate ($C_7H_6O_5$, MW = 188.14 with a purity of 98 %) was provided by PanReac. Potassium dichromate ($K_2Cr_2O_7$) 99.7 % and sulfuric acid 95 % were provided from Sigma Aldrich.

The natural clay is under the 'name Ghassoul Chorafa Al Akhdar' and from the company Sefrioui. The Olive stone is from the company 'Olea Food' in the region of Fez-Meknes.

2.2. Characterization of support and (HT-Gh-OS3 and HT-Gh-AC3) membrane

Fourier Transform Infrared (FTIR) analysis was performed using Fourier Transform Infrared Spectrometer (Shimadzu IRAffinity-1S). Termogravimetric (TGA-DTA) investigation was used by Shimadzu TA-60 type contraption. X-ray diffraction (XRD) analysis was performed by Philips PW 1800 instrument. The quickening voltage was 40 kV, the current was 20 mA, and the copper Kα radiation was $\lambda = 1.5418$ Å. Spectra of the different samples were registered in this range 2θ (5°–70°) with an accurate addition of 0.04°. The scanning electron microscope (SEM) of Quanta 200 from FEI Company in the research center of Moulay Ismail University of Meknes-Morocco, was used to determine the morphology of ceramic and membrane before and after filtration.

3. Membranes fabrication

3.1. Preparation of ceramics supports

The clay of Ghassoul 'Gh' was blended with 3 % of Olive stone (OS) or 3 % of actived carbon with a total mass of 4 g using the shaping technique using a mold under uniaxial pressure.

This mixture was spread in a stainless-steel mold then subjected to pressure of 10 tonnes in order to obtain raw supports in the form of pellets 2 mm thick and 4 cm in diameter. These supports were then subjected to sintering at 950C° according to a thermal program based on the thermogravimetric analysis of Ghassoul. The classical method was used to determine the porosity of the two ceramic supports (Qabaqous et al., 2018).

3.2. Deposed hydrotalcite onto ceramics supports

Both membranes deposited on the supports were carried out according to the hydrotalcite (HT) synthesis procedure, that is, the co-deposition method. Magnesium chloride ($MgCl_2 \cdot 6H_2O$) and aluminum chloride ($AlCl_3 \cdot 6H_2O$) are dissolved in 100 mL of distilled water (solution A) in such a way that the ratio of Mg to Al is 3. The mass of sodium

Fig. 1. Diagram of the laboratory pilot (1: pump, 2: solution tank, 3: pressure manometer, 4: valve, 5: sample holder module, 6: filtrate.

hydroxide 32 g (NaOH) and 2,12 g of sodium carbonate (Na_2CO_3) are also dissolved in 100 mL of distilled water (solution B). Drop by drop, these two solutions are added to a flask containing 20 mL of distilled water, keeping the pH between 9 and 10 at room temperature with magnetic stirring. The gel formed containing the Hydrotalcite particles was added drop by drop to the supports placed horizontally in a crystallizer. The product obtained was then brought to a temperature of 70 °C for 18 h in order to obtain a membrane deposit formed of a well-crystallized and well-spread layer on the surface of the ceramic support. After returning to room temperature, the membranes obtained are washed several times with distilled water to eliminate the free crystals not deposited on the surface of the support, and then dried at 80 °C.

4. Efficiency of OMWW purification

4.1. Preparation of OMWW samples

Olive mill wastewater samples were supplied by 2 phase system from Fez-Meknes region (Morocco). OMWW liquid samples were bubbled with nitrogen to avoid phenol degradation and filtered by centrifugation. Also, the samples diluted by distilled water with the following percentage (40 % OMW, 60 % OMW and 80 % OMW) to remove organic matter may be fouling the membrane.

4.2. Removal of polyphenols from olive mill wastewater onto membranes

Based on previous experiences (Singleton et al., 1999), all samples were filtered at different times ranging from 30 to 310 min using a pilot designed in the laboratory (Fig. 1), and the polyphenols before and after filtration was determined with the same protocol as in the previous study (Safae et al., 2020). The concentration of polyphenols was determined by a colorimetric method using Folin-Ciocalteu reagent that was cited in the same study (Safae et al., 2020).

4.3. Filtration pilot process

The pilot filtration system (Fig. 1) includes a 10 L of different dilution of OMW in the feed tank, a pump, two **manometers pressure** located before and after the flat-sheet membrane to measure the inlet and outlet pressure.

The conditional experience of filtration was used at temperature 25°C, the pression 1 bar like a previously study (Qabaqous et al., 2018), Safae et al., 2020).
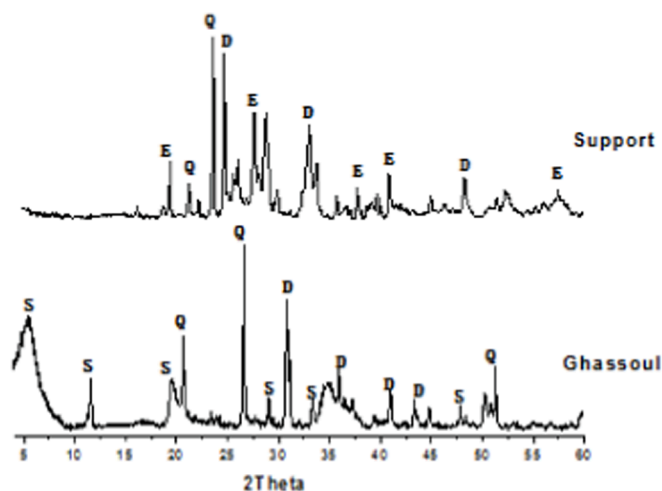
Fig. 2. X-ray diffractograms of raw Ghassoul 'Gh-B' and support S: stevensite, D: dolomite, Q: quartz, E: enstatite.

4.4. Measurement of membrane water permeability

The permeate flux of different samples was determined at different pressures (from 1 bar to 5 bar) and various times (from 30 min to180min), at constant temperature (25 °C).

After we calculated the flow at (25 °C) using the formular:

$$J = \frac{V}{A*t}$$

where: J is the flux (L.h^{-1}.m^{-2}), V is the volume (L) of water collected in period t (h), and A is the surface of the membrane, which is 8.04×10^{-4} m^2 in this case.

5. Results and discussion

5.1. Characterization of support

It is important to note that since the supports were obtained after sintering at 950 °C, the temperature at which the mineral or organic adjuvant is eliminated, and the deposed hydrotalcite onto both membranes, the characterizations by Infrared spectroscopy and X-ray diffraction of the two supports and membranes give the same spectra. Supports correspond to: Gh-AC3 and Gh-OS3 and membranes: HT-Gh-AC3 and HT-Gh-OS3.

5.1.1. X-ray-diffraction (XRD)

The X-ray diffractogram of Gh-B (Fig. 3) shows that crude Ghassoul

consists of three clay phases: The first phase is the stevensite 'S' phase, rays contained at 2θ = 5.70°, 11.61°, 19.33°, 29.43°, 33.40°, and 44.84°. The second phase is dolomitic phase 'D', lines included at 2θ = 30.83°, 34.58°, 41.03° and 35.22°. The third phase is 'Q' quartz phase where lines included at 2θ = 20.73°, 26.52° and 53.70°. 53.70°. We noticed the presence of free silica in the shape of quartz and dolomite in very small amounts. On the other hand, Stevensite is the magnesian pole of the series of smectites that make up the majority clay phase of Gh-B. These findings are consistent with previous work-based X/EDX fluorescence analyses (Allaoui et al., 2019), (Frost and Vassallo, 1996), (Ajbary et al., 2013), (Elass et al., 2011). After heating the support to 950 °C, the stevensite peaks disappeared, and the enstatite (E) peaks appeared. Also,
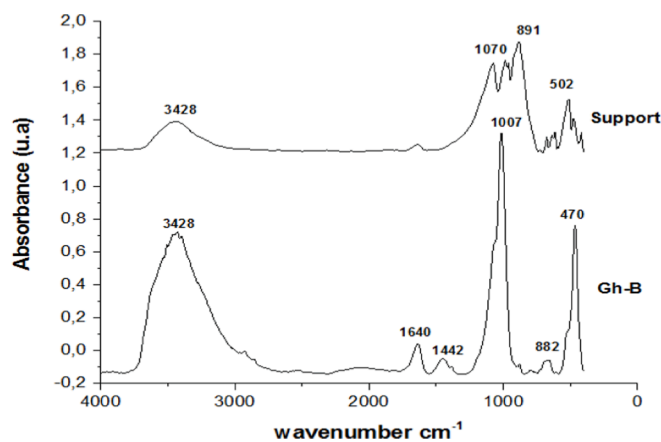
Fig. 4. IR spectra of Ghassoul and support.

Table 1
FTIR of Ghassoul powder (Gh-B) and support.

Frequency cm^{-1}	Bands of Gh-B	Bands of support
3428	Stretching vibrations of OH hydroxyl groups	Stretching vibrations of OH hydroxyl groups
1640	Deformation vibration of water molecules	Deformation vibration of water molecules
1442	Vibrations due to the presence of carbonates	–
1070	–	Stretching vibration of Al-OH group
1007–984	Asymmetric elongation vibrations of SiO$_2$	Asymmetric elongation vibrations of SiO$_2$
891–882	Deformation vibrations of (CO$_3$) and Al$_2$OH groups	Deformation vibration Al$_2$OH groups
502–470	Deformation vibrations of Si-O-Si bond	Deformation vibrations of Si-O-Si bond
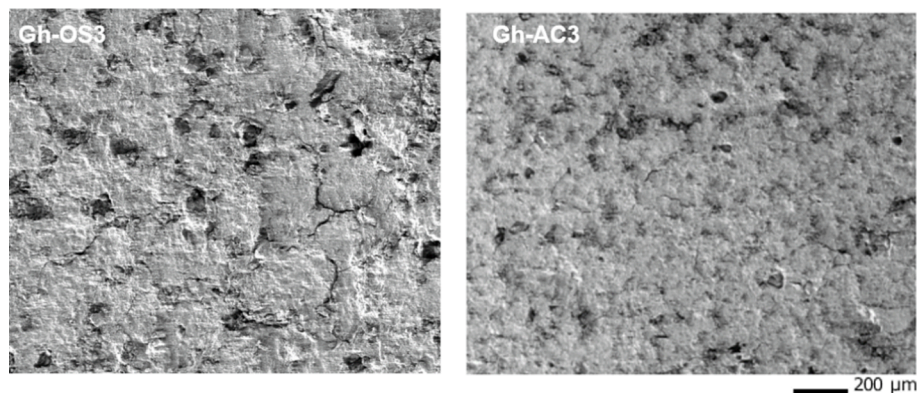
Fig. 3. Micrograph of supports (right) Gh-AC3, (left) Gh-OS3.
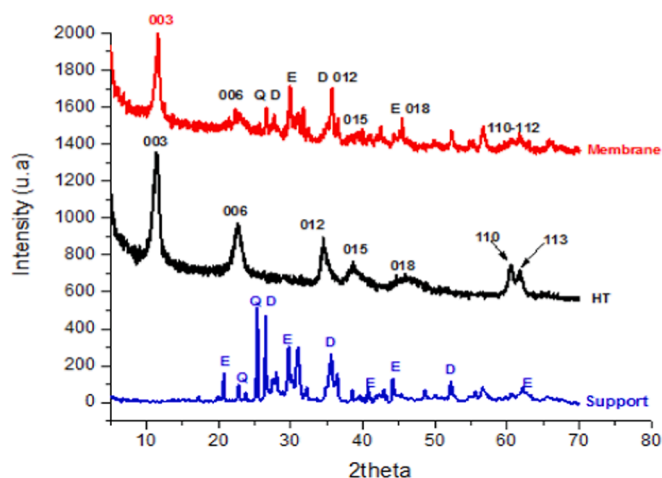
Fig. 5. X-ray diffractograms of support, Hydrotalcite and membrane.
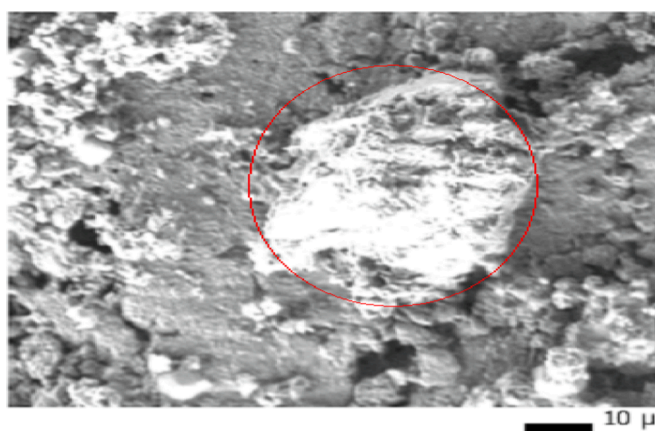
Fig. 6. Micrograms per SEM of membrane.

observe a displacement of the quartz lines and the dolomite with a decrease in their intensities; due to the change in the clay structure (ghassoul).

5.1.2. SEM and porosity

Scanning electron microscopy was used to examine the morphology, porosity of the prepared supports (Gh-OS3 and Gh-AC3) and visualize the surface defects.

Fig. 4 presents the micrographs of the supports Gh-OS3 and Gh-AC3, sintered at 950C that show dark zones, which constitute the pores, and grey zones presenting the clay matrix. Also, great porosity in support with olive stone as adjuvant Gh-OS3 than active carbon Gh-AC3. As a result, the organic adjuvant 'olive stone' after sintering gives a very porous support, compared to the one with the mineral adjuvant 'activated carbon'. The porosity was 31 % for olive stone and 27 % for activated carbon.

5.1.3. FTIR

Fig. 2 and Table 1 show infrared spectrum analysis for Gh-B (B = raw). The comparison between ghassoul and support is signified by the reduction of the intensity bands at 3428 cm^{-1} and 1640 cm^{-1} corresponding to the stretching and deformation vibrations of water molecules respectively and the disappearance of the band at 1442 cm^{-1} of the carbonate species. A new band at 1070 cm^{-1} corresponding to $Al_2(OH)_6$ group appeared. Also, a displacement of the asymmetric stretching vibration band of SiO_2 from 1007 to 984 cm^{-1} was observed.
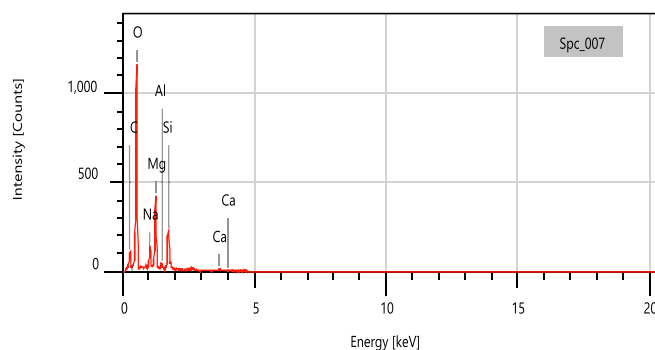
Fig. 7. EDX of membrane.
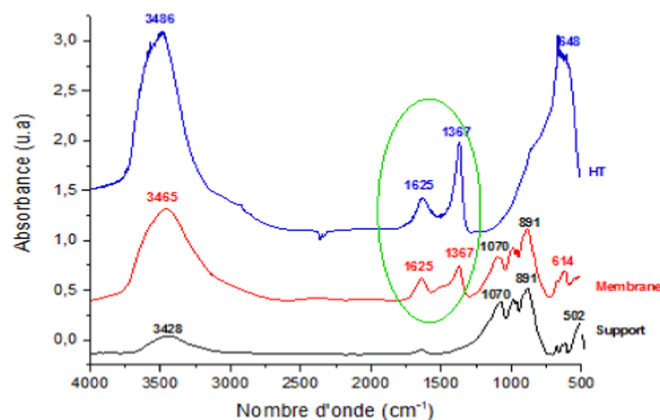
Fig. 8. Infrared spectra of support, Hydrotalcite and membrane.

6. Characterization of (HT-Gh-OS3 and HT-Gh-AC3) membranes

6.1. X-ray-diffraction

The diffractograms for both membranes and supports elaborated with 3 % olive stone Gh-OS3 or actived carbon Gh-AC3 as adjuvant show the same peaks as shown in Fig. 5. The diffractogram of the membrane (red color) indicates the presence of all the characteristic lines of the hydrotalcite phase and Ghassoul support. The fabrication protocol successfully deposed the hydrotalcite phase on the Ghasoul support and produced the HT-Gh-OS3 and HT-Gh-AC3 membranes.

6.2. SEM

A more or less significant agglomerate of particles of heterogeneous size in the form of flat sheets (platelets) is observed, which shows the presence of the hydrotalcite phase. We also note the presence of coating of the support surface by the hydrotalcite layer, which indicates the presence of membrane deposits (Fig. 7). These results confirm the idea of successful membrane production and corroborate those observed by XRD and FTIR.

6.3. Transmission electron microscopy coupled with energy dispersive analysis

EDX was used to confirm the membrane's elaboration, as shown in (Fig. 8). Elements C, O, Si, Na, Ca, Mg, and Al are shown as components of hydrotalcite and Ghassoul, confirming the presence of hydrotalcite (Mg, Al, C, and O) and Ghassoul (Si, Na, and O) phases in the membranes based on XRD and FTIR results.
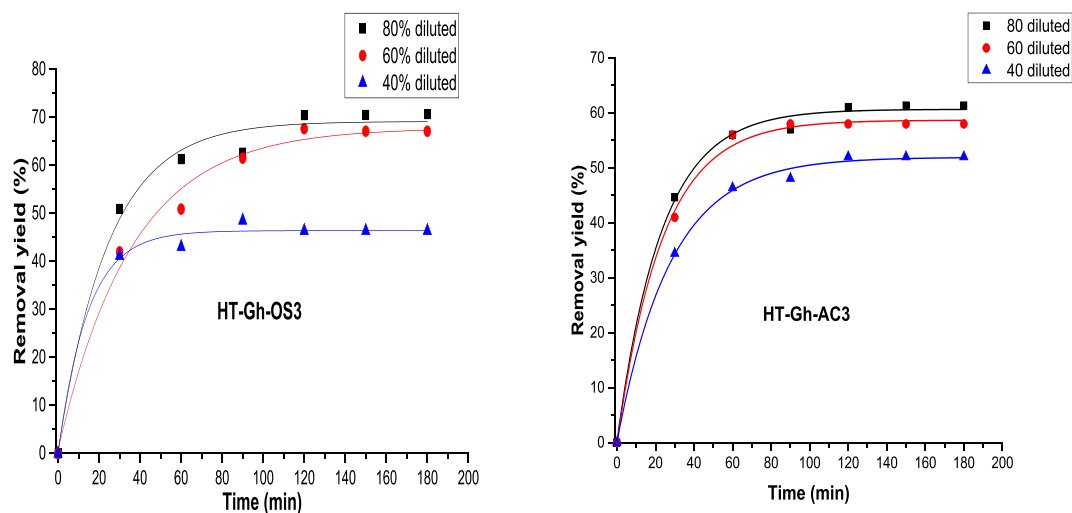
Fig. 9. Removal efficiency as a function of time.
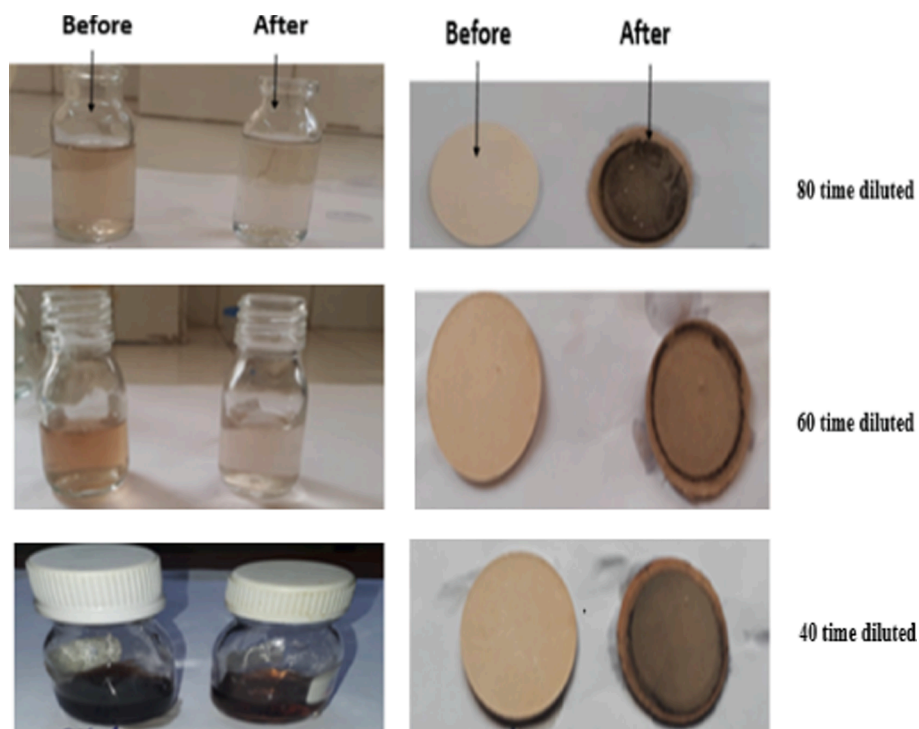
Fig. 10. Photos of olive mill wastewater solutions (left) and the HT- Gh-OS3 membrane (right) before and after filtration of olive mill wastewater at different dilution rates.

6.4. FTIR

Fig. 6 presents the infrared spectra of the hydrotalcite HT, the support, and the membrane. The infrared spectrum of the membranes shows the principal bands that are characteristics of hydrotalcite and ghassoul phases. It is observed that the bands at 1625 cm^{-1} and 1370 cm^{-1} are associated with water and carbonate species for hydrotalcite HT. The presence of bands at 1070 cm^{-1}, 891 cm^{-1} corresponds to the ghassoul phase. The band of O–H groups at 3465 cm^{-1} is broad, gathering hydrotalcite and ghassoul hydroxyl species. These results confirm the membrane deposition, which is in agreement with the XRD observations.

7. Removal of polyphenols from olive mill wastewater onto membranes

Fig. 9 shows the evolution of polyphenol retention as a function of time for the two membranes, HT-Gh-OS3 and HT-Gh-AC3, at different dilutions of olive mill wastewater. A rapid increase in retention is noted during the first 20 min. In contrast, the tendency decreases significantly in speed with time to tend towards stabilization after 120 min for the two types of membranes and all dilutions. The stabilization is due to the clogging of the membrane by the presence of deposits of polyphenolic compounds on the surface of the membrane. The results of the filtration experiments show the different dilutions of olive mill wastewater (40, 60 and 80 time) before and after filtration for the HT-Gh-OS3 membrane (Fig. 10) and the olive mill wastewater diluted 80 times for the HT-Gh-
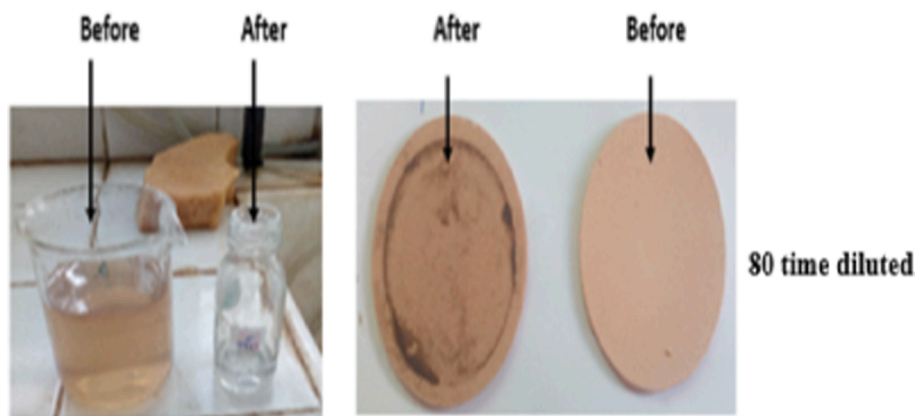
Fig. 11. Photos of olive mill wastewater solutions (left) HT- Gh-AC3 membrane (right) before and after filtration of olive mill wastewater diluted to 80%.
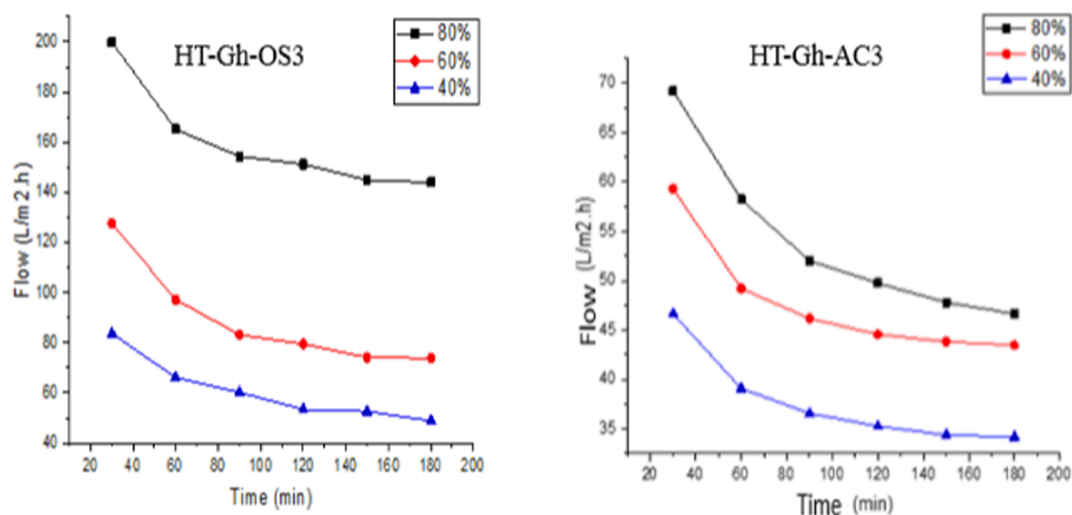
Fig. 12. Evolution of the flux as a function of time for the two elaborate membranes.

AC3 membrane (Fig. 11).

The photos of filtration experiments before and after filtration for the different dilutions of olive mill wastewater, 40, 60 and 80 time with HT-Gh-OS3 membrane and 80 times with HT-Gh-AC3 membrane, are presented in Fig. 10 and Fig. 11 respectively.

As shown in (Figs. 10 and 11), polyphenols retention by HT-Gh-OS3 and HT-Gh-AC3 membranes decreased color for all diluted samples, as mentioned by Qabaqous et al. in the retention of heavy metal Cr on the hydrotalcite based on ghassoul and activated carbon membrane Mg3Al-Gh-AC3 (Qabaqous et al., 2018). However, olive mill wastewater diluted
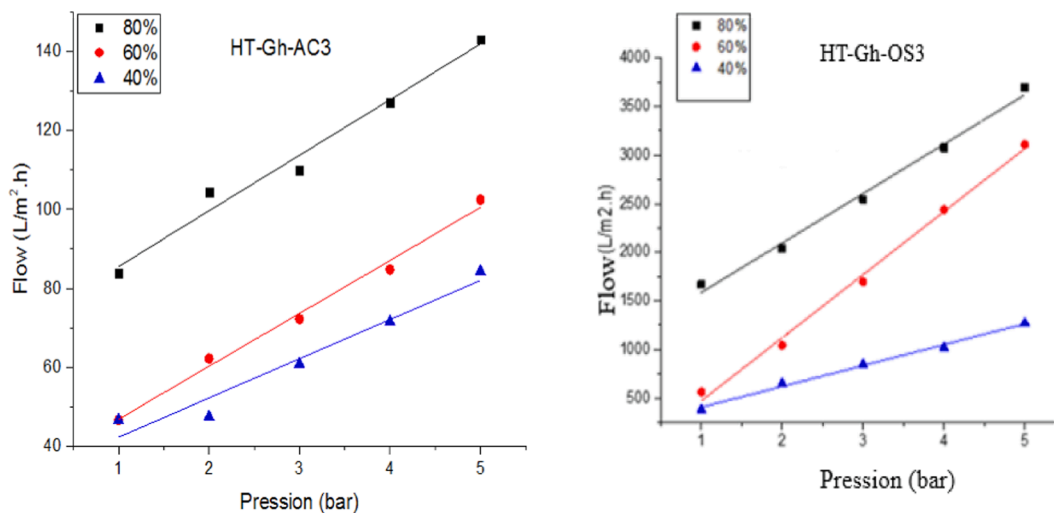
Fig. 13. Evolution of the flow according to the pressure for the two elaborate membranes.
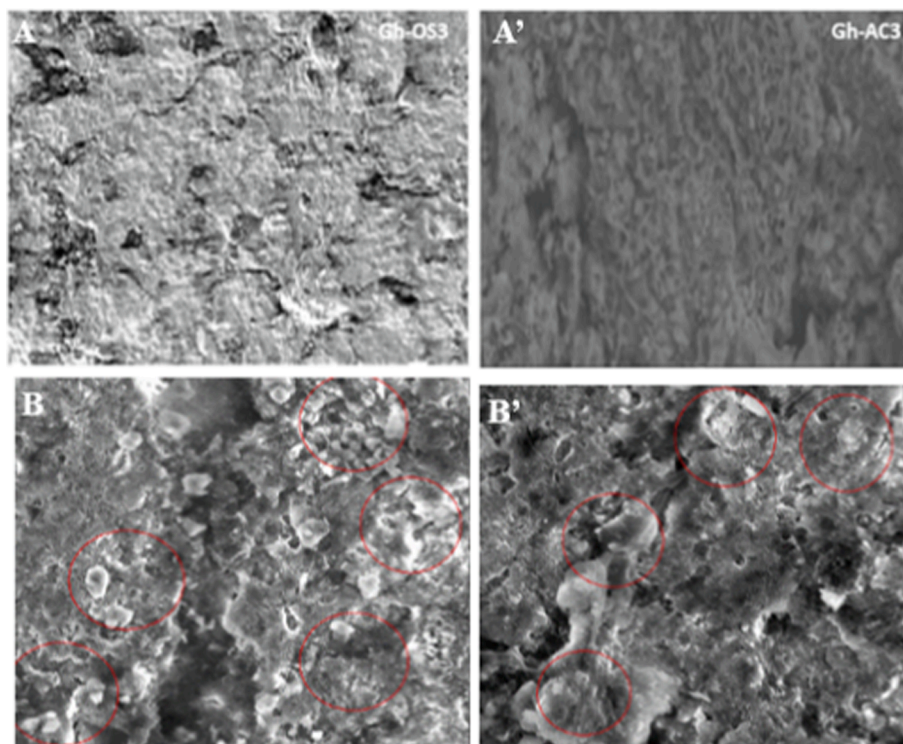
Fig. 14. Morphology of the membrane (A, A') before and (B, B') after the filtration tests.

to 80 % provides high polyphenol removal efficiency, equal to 71 % and 60 % for olive stone and activated carbon membrane, respectively, and one bar filtration pressure (Fig. 9). Based on current results and comparison of our previous studies for the adsorption of polyphenols onto ghassoul, that filtration membrane makes to retain a greater quantity of polyphenols than that obtained by the adsorption process (Qads = 161 mg/g, i.e., a polyphenol removal efficiency of 53 % (Allaoui et al., 2019). In addition, the current results are better than Macro Stoller et al., who found a removal efficiency of polyphenol of 55 % using a filtration pressure equal to five bars (Stoller 2008). Therefore, the membrane process is interesting compared to the adsorption method in eliminating polyphenols from olive mill wastewater.

7.1. Measurement of membranes HT-Gh-OS3 and HT-Gh-AC3 water permeability

The Fig. 12 shows the flow a function of time for two membrane. At the beginning we observed a decrease in flow until a stabilization after 120 min of filtration where a dilution rate of 80 %, the HT- Gh-OS3 membrane flux goes from 199 L/m^2.h (t = 30 min) to 143 L/m^2.h (t = 120 min), and for HT-Gh-AC3 this flow goes from 69 (t = 30 min) to 46 L/m^2.h (t = 120 min). Similarly, for the other dilutions, the flux value for the HT-Gh-OS3 membrane is greater than that of HT-Gh-AC3 (Fig. 12). In conclusion, the filtration through the HT-Gh-OS3 membrane is more important than HT-Gh-AC3, and this membrane also shows less clogging. Therefore, the HT-Gh-OS3 membrane can be used to remove polyphenols at a larger size than in the laboratory or even on an industrial scale.

The mechanical resistance of each membrane was checked by determining its permeability as a function of the pressure for all dilutions (80 %, 60 %, and 40 %) and varying the pressures from 1 to 5 bars. Fig. 13 represents the linear variation of the permeate flux J(L/h. m2) as a function of the applied transmembrane pressure (bar) for the different dilutions. J value for the 80 % olive mill wastewater is greater than that of the 60 % and 40 % olive mill wastewater in the case of the two membranes. The flux increases with the increase in pressure for all

dilutions of the olive mill wastewater. During these experiments, it was found that the increase in pressure up to 5 bars does not lead to the cracking of the membranes, which makes it possible to conclude that the two membranes have good mechanical resistances. These results are in agreement with the work of E. Turano et al., who studied the treatment of olive mill wastewater by an integrated centrifugation-ultrafiltration system with a commercial membrane (Turano et al., 2002).

7.2. Characterization of membranes after filtration

7.2.1. SEM of the membrane after filtration

The morphology of the membrane before the filtration operation shows the formation of a layer of hydrotalcite in the form of stratified sheets constituting the deposit on the surface of the support (Fig. 14A and A'). This hydrotalcite layer deposition reduces the pore size of the 'Ghassoul' support, and the membrane surface becomes denser. After filtration (Fig. 14 B and B'), dense layers forming the deposit of polyphenols from olive mill wastewater on the membrane were observed. It indicates that the polyphenols were retained by the membrane and confirmed the deposition of polyphenol species on the membrane, as shown in (Figs. 10 and 11).

8. Conclusion

The elaboration of the membrane filtration based on natural Ghassoul clay and olive stone has been successfully carried as the activated carbon membrane out to eliminate polyphenols from the wastewater of oil mills. The Different dilutions of OMW (40 %, 60 %, and 80 %) were filtered by the two membranes using a filtration pilot. The result shows that the efficiency of elimination of polyphenol species is 71 % for the membrane with olive stone and 61 % with activated carbon membrane. This shows that the organic matter (olive stone) gives a good porosity to the membrane against the activated carbon. Retention of polyphenols was confirmed by SEM and maybe the future method for the removal of these species.

Declaration of Competing Interest

The authors declare that they have no known competing financial interests or personal relationships that could have appeared to influence the work reported in this paper.

Acknowledgement

References

Ajbary, M., Santos, A., Morales-flórez, V., Esquivias, L., 2013. Applied Clay Science Removal of basic yellow cationic dye by an aqueous dispersion of Moroccan stevensite. Appl. Clay Sci. 80–81, 46–51. https://doi.org/10.1016/j.clay.2013.05.011.

Al Aani, S., Mustafa, T.N., Hilal, N., 2020. Ultrafiltration membranes for wastewater and water process engineering: A comprehensive statistical review over the past decade. J. Water Process Eng. 35, 101241.

Allaoui S, Bennani MN, Ziyat H, et al (2019) Remove of polyphenols on a natural clay " Ghassoul " and effect of the adsorption on the physicochemical parameters of the olive mill wastewaters. 6:40–46.

Azzam,Olive mills wastewater treatment using mixed adsorbents of volcanic tuff, natural clay and charcoal. Journal of Environmental Chemical Engineering 6 (2018) 2126–2136.

Berbel, J., Posadillo, A., 2018. Review and analysis of alternatives for the valorisation of agro-industrial olive oil by-products. Sustainability 10, 237. https://doi.org/10.3390/su10010237.

Bilal, R.M., Liu, C., Zhao, H., Wang, Y., Farag, M.R., Alagawany, M., Hassan, F.U., Elnesr, S.S., Elwan, H.A.M., Qiu, H., Lin, Q., 2021. Olive oil: Nutritional applications, beneficial health aspects and its prospective application in poultry production. Front. Pharmacol. 25 (12), 723040 https://doi.org/10.3389/fphar.2021.723040.

Chiavola et al., Biological treatment of olive mill wastewater in a sequencing batch reactor. Biochemical Engineering Journal 85 (2014) 71–78.

Di Giacomo, G., Romano, P., 2022. Evolution of the olive oil industry along the entire production chain and related waste management. Energies 15 (2), 465. https://doi.org/10.3390/en15020465.

Elass, K., Laachach, A., Alaoui, A., Azzi, M., 2011. Applied Clay Science Removal of methyl violet from aqueous solution using a stevensite-rich clay from Morocco. Appl. Clay Sci. 54, 90–96. https://doi.org/10.1016/j.clay.2011.07.019.

Flores et al., Treatment of olive oil mill wastewater by single electrocoagulation with different electrodes and sequential electrocoagulation/electrochemical Fenton-based processes. Journal of Hazardous Clay s 347 (2018) 58–66.

Galanakis, C.M., Tsatalas, P., Galanakis, I.M., 2018. Implementation of phenols recovered from olive mill wastewater as UV booster in cosmetics. Ind. Crop. Prod. 111, 30–37.

Gebreyohannes et al., Treatment of olive mill wastewater by forward osmosis. Separation and Purification Technology 147 (2015) 292-302.

Qabaqous O, Bennani MN, Tijani N, et al (2018) Removal of hexavalent Chromium by Ghassoul Hydrotalcites Membranes (GHTM). 2508:2511–2519.

Rodriguez, G., Lama, A., Rodriguez, R., Jiménez, A., Guillen, R., Fernandez-Bolanos, J., 2008 Sep. Olive stone an attractive source of bioactive and valuable compounds. Bioresour. Technol. 99 (13), 5261–5269. https://doi.org/10.1016/j.biortech.2007.11.027.

Safae, A., Mohammed, N.B., Hamid, Z., et al., 2020. Removing polyphenols contained in olive mill wastewater by membrane based on natural clay and hydrotalcite Mg-Al. Moroccan J. Chem. 8, 318–325.

Sani, S., Dashti, A.F., Adnan, R., 2020. Applications of Fenton oxidation processes for decontamination of palm oil mill effluent: A review. Arab. J. Chem. 13 (10), 7302–7323. https://doi.org/10.1016/j.arabjc.2020.08.009.

Sciascia, L. Casella, S. Cavallaro, G. Lazzara, G. Milioto, S. Princivalle, F. Parisi, F. Olive mill wastewaters decontamination based on organo-nano-clay composites, Ceramics Inter. (2019). 45(2)-part B. 2751-2759. https://doi.org/10.1016/j.ceramint.2018.08.155.

Sciubba F, Chronopoulou L, Pizzichini D, Lionetti V, Fontana C, Aromolo R, Socciarelli S, Gambelli L, Bartolacci B, Finotti E, Benedetti A, Miccheli A, Neri U, Palocci C, Bellincampi D. Olive Mill Wastes: A Source of Bioactive Molecules for Plant Growth and Protection against Pathogens. Biology (Basel) 2020 6;9(12):450. doi: 10.3390/biology9120450.

Singleton, V.L., Orthofer, R., Lamuela-Raventós, R.M., 1999. [14] Analysis of total phenols and other oxidation substrates and antioxidants by means of folin-ciocalteu reagent. Methods Enzymol. 299, 152–178. https://doi.org/10.1016/S0076-6879(99)99017-1.

Stoller M (2008) Technical optimization of a dual ultrafiltration and nanofiltration pilot plant in batch operation by means of the critical flux theory : A case study. 47: 1165–1170. doi: 10.1016/j.cep.2007.07.012.

Tapia-Quirós, P., Montenegro-Landívar, M.F., Reig, M., Vecino, X., Saurina, J., Granados, M., Cortina, J.L., 2022. Integration of nanofiltration and reverse osmosis technologies in polyphenols recovery schemes from winery and olive mill wastes by aqueous-based processing. Membranes 12 (3), 339.

Terral, J.-F., Bonhomme, V., Pagnoux, C., Ivorra, S., Newton, C., Paradis, L., Ater, M., Kassout, J., Limier, B., Bouby, L., Cornet, F., Barazani, O., Dag, A., Galili, E., 2021. The shape diversity of olive stones resulting from domestication and diversification unveils traits of the oldest known 6500-years-old table olives from Hishuley Carmel Site (Israel). Agronomy 11 (11), 2187. https://doi.org/10.3390/agronomy11112187.

Turano E, Curcio S, Paola MG De, et al (2002) An integrated centrifugation – ultrafiltration system in the treatment of olive mill wastewater. 209:519–531.

Further reading

Frost Rayl, Vassallo Am (1996) The dehydration of the kaolinite clay mineral using infrared emission spectroscopy. 44:635-651.

Kontos et al., Implementation of membrane filtration and melt crystallization for the effective treatment and valorization of olive mill wastewaters. Separation and Purification Technology 193 (2018) 103–111.

Lee S. Z., Chin. S. Y., Lim. J, W., Witoon, T., Cheng C. K., Treatment technologies of palm oil mill effluent (POME) and olive mill wastewater (OMW): A brief review, Environmental Technology & Innovation, 2019, 15, 100377. https://doi.org/10.1016/j.eti.2019.100377.